J|A|C|S
ARTICLES
Published on Web 09/19/2003

Crystal Environments Probed by EPR Spectroscopy. Variations in the EPR Spectra of Co^{II}(octaethylporphyrin) Doped in Crystalline Diamagnetic Hosts and a Reassessment of the Electronic Structure of Four-Coordinate Cobalt(II)

Andrew Ozarowski,† Hon Man Lee, and Alan L. Balch*

Contribution from the Department of Chemistry, University of California, Davis, California 95616

Received April 11, 2003; Revised Manuscript Received July 8, 2003; E-mail: albalch@ucdavis.edu

Abstract: The powder and single-crystal EPR spectra of Co^{II}(OEP) (OEP is the dianion of octaethylporphyrin) doped into a range of diamagnetic crystals including simple four-coordinate hosts, H_2(OEP), the triclinic B form of Ni^{II}(OEP), the tetragonal form of Ni^{II}(OEP) and Zn^{II}(OEP); five-coordinate hosts, (μ-dioxane)-{Zn^{II}(OEP)}$_2$ and (py)Zn^{II}(OEP); six-coordinate hosts, (py)$_2Zn^{II}$(OEP) and (py)$_2Mg^{II}$(OEP); and hosts containing fullerenes, C_{60}·2Zn^{II}(OEP)·$CHCl_3$, C_{70}·Ni^{II}(OEP)·C_6H_6·$CHCl_3$, and C_{60}·Ni^{II}(OEP)·2C_6H_6 have been obtained and analyzed. Spectra were simulated using a program that employed the exact diagonalization of the 16 × 16 complex spin Hamiltonian matrix. The EPR spectra of these doped samples are very sensitive to the environment within each crystal with the crystallographic site symmetry determining whether axial or rhombic resonance patterns are observed. For Co^{II}(OEP) doped into tetragonal Ni^{II}(OEP) (which displays a very large $g_\perp$ of 3.405 and a very small $g_\parallel$ of 1.544) and several other crystals containing four-coordinate metal sites, the g components could not be fit using existing theory with the assumption of the usual z^2 ground state. However, reasonable agreement of the observed EPR parameters could be obtained by assuming that the unpaired electron resides in an xy orbital in the four-coordinate complexes.

Introduction

The EPR spectra of cobalt(II) porphyrins are sensitive to their environment, and this sensitivity renders them useful as probes of the internal sites within crystals. Previous work has shown that cobalt porphyrins such as Co^{II}(OEP) (for structure, see Chart 1) exhibit distinct EPR parameters that are indicative of their coordination geometry and the presence and nature of the axial ligands.[1−3] Four-coordinate cobalt(II) complexes of symmetrical porphyrins such as tetraphenylporphyrin (H_2TPP) and octaethylporphyrin (H_2OEP) typically exhibit spectra with a very high g_x, $g_y > 3$, and a small g_z of <1.7 when doped into lattices that exclude the possibility of axial coordination. However, these parameters change to g_x, $g_y < 2.5$, and $g_z > 2$ when axially coordinated ligands are present. Such spectra have typically been recorded from samples in glassy media such as frozen toluene solutions at 77 K, and the spectral resolution has been found to be influenced by the solvents used to prepare the glasses. Hyperfine splittings from cobalt and axially coordinated nitrogen atoms are generally observable in the spectra.[1,2,4] Hyperfine couplings from the in-plane nitrogen atoms of the porphyrin have recently been observed in a pulsed EPR study of Co^{II}(TPP) doped in Zn^{II}(TPP),[5] but were found to be smaller by a factor of 4 than the value predicted on the basis of an electronic structure with the unpaired electron in the z^2 orbital.[6] In the presence of dioxygen and an axial nitrogen donor, six-coordinate adducts are formed with a reduced spread of g values and an inversion of the magnitudes of g_x, g_y, and g_z so that g_x, $g_y \approx 2.0$, and $g_z \approx 2.07$.[1,2,7,8] The presence of π-donors such as 1,3,5-trimethoxybenzene and pyrene and π-acceptors such as 1,3,5-trinitrobenzene and 2,4,5,7-tetranitrofluorenone have also been shown to affect the nature of the EPR spectra of Co^{II}(p-tolylporphyrin) in toluene glasses. The effects include lowering of g_x and g_y (relative to the value in Co^{II}(p-tolylporphyrin) itself)

Chart 1

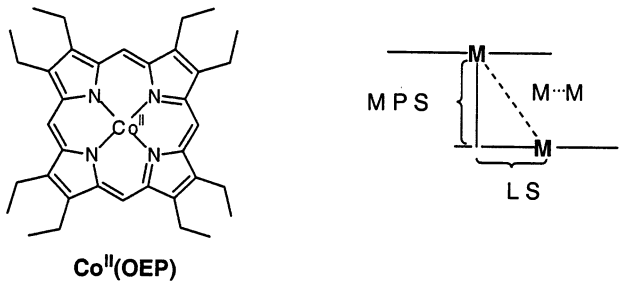

Co^{II}(OEP)

† Permanent address: Department of Chemistry and Department of Pharmacology, The University of Florida, P.O. Box 118440, Gainesville, FL 32611-8440.

(1) Walker, F. A. *J. Am. Chem. Soc.* **1970**, *92*, 4235.
(2) Walker, F. A. *J. Magn. Reson.* **1974**, *15*, 201.
(3) Iwaizumi, M.; Ohba, Y.; Iida, H.; Hirayama, M. *Inorg. Chim. Acta* **1984**, *82*, 47.
(4) Van Doorslaer, S.; Schweiger, A. *J. Phys. Chem. A* **1999**, *103*, 5446.
(5) Van Doorslaer, S.; Schweiger, A. *Phys. Chem. Chem. Phys.* **2001**, *3*, 159.
(6) McGarvey, B. R. *Can. J. Chem.* **1975**, *53*, 2498.
(7) Van Doorslaer, S.; Schweiger, A. *J. Phys. Chem. B* **2000**, *104*, 2919.
(8) Van Doorslaer, S.; Zingg, A.; Schweiger, A.; Diederich, F. *ChemPhysChem* **2002**, *3*, 659.

10.1021/ja030221f CCC: $25.00

and increasing of g_z, along with reduction of the A_x, A_y, and A_z values that arise from coupling to cobalt.[1−3]

Within crystals, the EPR spectra of a probe molecule like Co^{II}(OEP) can be expected to be sensitive to the crystallographic symmetry of the host, which need not have the four-fold symmetry associated with the probe itself, and the nature of neighboring molecules. Moreover, crystal packing forces within the crystal environment may serve to distort the intrinsic geometry of the probe molecule. Crystal packing forces have frequently been invoked to explain anomalous features in the crystal structures of individual molecules. For example, crystal packing forces have been proposed to cause changes in the coordination modes of ligands ($^1\eta$ or $^2\eta$ coordination of benzyl groups,[9] $^3\eta$ or $^4\eta$ coordination by bis(sulfonamido)bis(amide) ligands[10]), the nonplanarity of [*N*]phenylenes[11] and of copper(II) amino acid complexes,[12] and details of the DNA helix structure.[13,14]

Here, we report on our investigation of crystals in which Co^{II}(OEP) was doped into a series of diamagnetic M^{II}(OEP) hosts with known crystal structures. These diamagnetic hosts include four-, five-, and six-coordinate complexes. Additionally, molecules of M^{II}(OEP) can readily cocrystallize with the fullerenes, C_{60} or C_{70}.[15,16] These solids contain close contacts between the porphyrin and the fullerene and present an opportunity to examine the effects of neighboring fullerenes on the spectral characteristics of Co^{II}(OEP). The components of the hyperfine and *g* tensors of Co^{II}(OEP) were found from simulation procedures for both powder and single-crystal spectra and were interpreted according to theoretical methods developed by McGarvey[6] and by Lin.[17−20]

Results

The Structures of Host Crystals and Comparisons with Those of the Guest Molecule, Co^{II}(OEP). Crystallographic data on a set of diamagnetic Ni^{II}(OEP)- and Zn^{II}(OEP)-containing solids are set out in Table 1. These compounds include four hosts (H_2(OEP),[21] the triclinic B form of Ni^{II}(OEP),[22] the tetragonal form of Ni^{II}(OEP),[23] and Zn^{II}(OEP)), that provide an environment for a simple four-coordinate guest. The triclinic B form of Ni^{II}(OEP), Zn^{II}(OEP), and Co^{II}(OEP) are isostructural, while the structures of the other two differ. The structure of Zn^{II}(OEP) is reported here for the first time. The structure of H_2(OEP), like that of the isostructural series, the triclinic B form of Ni^{II}(OEP), Zn^{II}(OEP), and Co^{II}(OEP), contains a planar, centrosymmetric porphyrin, but with less overlap of the π-system of adjacent macrocycles.

The interactions between adjacent porphyrins have been described by Scheidt and Lee in terms of the parameters M···M, the metal−metal separation; M.P.S., the mean plane separation; and L.S., the lateral shift, which are shown for a pair of metalloporphyrins in a side-on orientation in Chart 1.[24] For H_2(OEP), all of these parameters are greater than the corresponding parameters for the triclinic B forms of the

Table 1. Crystallographic Parameters for Hosts

	H_2OEP[a]	Ni^{II}(OEP)[b] triclinic B	Ni^{II}(OEP)[c] tetragonal	Zn^{II}(OEP)[d] (triclinic B)
space group	$P\bar{1}$	$P\bar{1}$	$I4_1/a$	$P\bar{1}$
number of porphyrin sites	1	1	1	1
porphyrin symmetry		*i*	$\bar{4}$	*i*
M−N (Å)		1.946(4)	1.929	2.035(2)
		1.958(4)		2.036(2)
M···N (Å)				
M···C (Å)				
M···M (Å)		4.802	8.228	4.692
Ct···Ct (Å)	7.483	4.802	8.228	4.692
M.P.S. (Å)		3.44		3.34
L.S. (Å)	6.60	3.35	7.47	3.30
ΔM−N_4 plane (Å)		0		0

	(μ-dioxane)-{Zn^{II}(OEP)}$_2$[d]	(py)Zn^{II}(OEP)[e]	(py)$_2Zn^{II}$(OEP)[d]	(py)$_2Mg^{II}$(OEP)[f]
space group	$P2_1/n$	$P\bar{1}$	$P\bar{1}$	$P\bar{1}$
number of porphyrin sites	1	1	1	1
porphyrin symmetry	none	none	*i*	*i*
M−N (Å)	2.051(2)	2.068(3)	2.064(2)	2.064(2)
	2.046(2)	2.062(3)	2.066(2)	2.0752
	2.042(2)	2.061(3)		
	2.055(2)	2.075(3)		
M···N (or O) (Å)	2.240(2)	2.200(3)	2.402(2)	2.389(2)
M···C (Å)				
M···M (Å)	3.799	8.217	9.856	9.567
Ct···Ct (Å)	3.678	7.806	9.856	9.567
M.P.S. (Å)	3.244	5.08	8.28	8.15
L.S. (Å)	1.98	6.46	5.36	5.00
ΔM−N_4 plane (Å)	0.105	0.31	0	0

	C_{60}·2Zn^{II}(OEP)·$CHCl_3$[g]	C_{70}·Ni^{II}(OEP)·C_6H_6·$CHCl_3$[g]	C_{60}·Ni^{II}(OEP)·2C_6H_6[h]
space group	$P2_12_12_1$	$P\bar{1}$	
number of metal sites	2	1	1
site symmetry	none	none	none
M−N (Å)	2.089(4) 2.042(5)	1.950(6)	1.948
	2.054(5) 2.081(5)	1.956(6)	1.949
	2.030(4) 2.047(5)	1.956(6)	1.955
	2.036(5) 2.033(4)	1.960(6)	1.952
M···N (Å)	2.592 2.674	3.152	4.101
M···C (Å)	2.944 2.984	2.836	3.004
M···M (Å)	3.166 37°	3.485	4.685
Ct···Ct (Å)	3.68	3.65	4.706
M.P.S. (Å)	3.21	3.28	3.497
L.S. (Å)	1.80	1.60	3.173
Δ M−N_4 plane (Å)	0.1605 0.1402	0.0276	0.013

[a] Lauher, J. W.; Ibers, J. A. *J. Am. Chem. Soc.* **1973**, *95*, 5148. [b] Brennan, T. D.; Scheidt, W. R.; Shelhutt, J. A. *J. Am. Chem. Soc.* **1988**, *110*, 3919. [c] Meyer, E. F. *Acta Crystallogr., Sect. B* **1972**, *28*, 2162. [d] This work. [e] Cullen, D. L.; Meyer, E. F. *Acta Crystallogr., Sect. B* **1976**, *32*, 2259. [f] Bonnett, R.; Hursthouse, M. B.; Malik, K. M. A.; Marteen, B. *J. Chem. Soc., Perkin Trans. 2* **1997**, 2072. [g] Olmstead, M. M.; Costa, D. A.; Maitra, K.; Noll, B. C.; Phillips, S. L.; Van Calcar, P. M.; Balch, A. L. *J. Am. Chem. Soc.* **1999**, *121*, 7090. [h] Lee, H. M.; Olmstead, M. M.; Suetsuna, T.; Shimotani, H.; Dragoe, N.; Cross, R. J.; Kitazawa, K.; Balch, A. L. *Chem. Commun.* **2002**, 1352.

(9) Giesbrecht, G. R.; Whitener, G. D.; Arnold, J. *Organometallics* **2000**, *19*, 2809.
(10) Pritchett, S.; Gantzel, P.; Walsh, P. J. *Organometallics* **1997**, *16*, 5130.
(11) Holmes, D.; Kumaraswamy, S.; Matzger, A. J.; Vollhardt, K. P. C. *Chem.-Eur. J.* **1999**, *5*, 3399.
(12) Sabolovic, J.; Liedl, K. R. *Inorg. Chem.* **1999**, *38*, 2764.
(13) Dickerson, R. E.; Goodsell, D. S.; Neidle, S. *Proc. Natl. Acad. Sci. U.S.A.* **1994**, *91*, 3579.
(14) Skrynnikov, N. R.; Goto, N. K.; Yang, D.; Choy, W.-Y.; Tolman, J. R.; Mueller, G. A.; Kay, L. E. *J. Mol. Biol.* **2000**, *295*, 1265.
(15) Olmstead, M. M.; Costa, D. A.; Maitra, K.; Noll, B. C.; Phillips, S. L.; Van Calcar, P. M.; Balch, A. L. *J. Am. Chem. Soc.* **1999**, *121*, 7090.
(16) Ishii, T.; Aizawa, B. N.; Yamashita, M.; Matsuzaka, H.; Kodama, T.; Kikuchi, K.; Ikemoto, I.; Iwasa, Y. *J. Chem. Soc., Dalton Trans.* **2000**, 4407.
(17) Lin, W. C. *Mol. Phys.* **1976**, *31*, 657.
(18) Lin, W. C. *Inorg. Chem.* **1976**, *15*, 1114.
(19) Lin, W. C. *Inorg. Chem.* **1980**, *19*, 1072.
(20) Lin, W. C. *J. Magn. Reson.* **1986**, *68*, 146.
(21) Lauher, J. W.; Ibers, J. A. *J. Am. Chem. Soc.* **1973**, *95*, 5148.
(22) Brennan, T. D.; Scheidt, W. R.; Shelnutt, J. A. *J. Am. Chem. Soc.* **1988**, *110*, 3919.
(23) Meyer, E. F., Jr. *Acta Crystallogr.* 1**972**, *B28*, 2162.
(24) Scheidt, W. R.; Lee, Y. J. *Struct. Bonding (Berlin)* **1987**, *64*, 1.

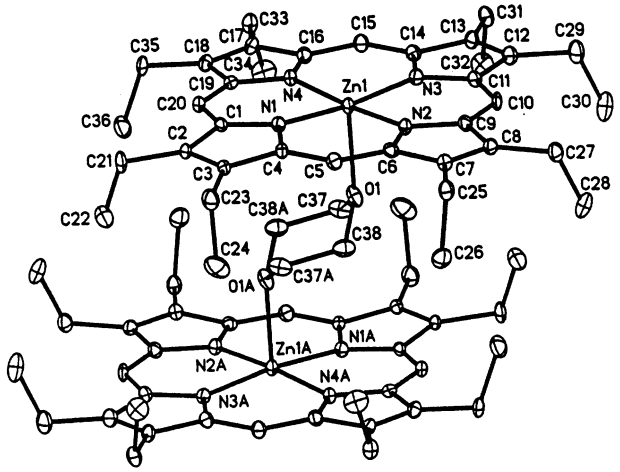

Figure 1. A perspective view of (μ-dioxane){Zn^{II}(OEP)}$_2$ which shows the encapsulation of the bridging dioxane portion. Thermal contours are shown at the 50% level. Selected bond distances (Å): Zn(1)−N(1), 2.053(3); Zn(1)−N(2), 2.042(3); Zn(1)−N(3), 2.044(4); Zn(1)−N(4), 2.068(3); Zn(1)−O, 2.241(2). Selected bond angles (deg): N(1)−Zn−N(2), 89.80(13); N(1)−Zn−N(3), 172.91(10); N(1)−Zn−N(4), 89.52(14); N(2)−Zn−N(3), 90.26(14); N(2)−Zn−N(4), 175.39(12); N(3)−Zn−N(4), 89.85(15); N(1)−Zn−O, 94.67(12); N(2)−Zn−O, 90.95(10); N(3)−Zn−O, 92.42(12); N(4)−Zn−O, 93.65(10).

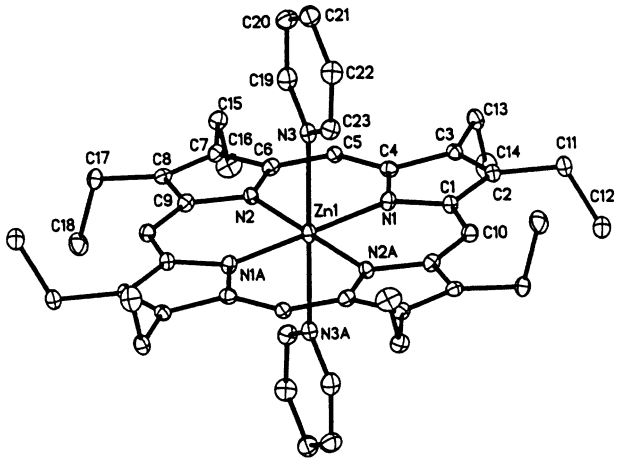

Figure 2. The molecular structure of (py)$_2$$Zn^{II}$(OEP) with thermal contours at the 50% level for all non-hydrogen atoms. Selected bond distances (Å): Zn(1)−N(1), 2.0652(13); Zn(1)−N(2), 2.0675(13); Zn(1)−N(3), 2.4039(14). Selected bond angles (deg): N(1)−Zn−N(2), 89.73(5); N(1)−Zn−N(2′), 90.27(5); N(1)−Zn−N(3), 88,25(5); N(2)−Zn−N(3), 91.96(5).

Table 2. Crystallographic Parameters for Guests

	Co^{II}(OEP)[a]	C_{60}·2Co^{II}(OEP)·$CHCl_3$[b]	C_{70}·Co^{II}(OEP)·C_6H_6·$CHCl_3$[b]
space group	$P\bar{1}$	$P2_12_12_1$	$P\bar{1}$
number of porphyrin sites	1	2	1
porphyrin symmetry	i	none	none
M−N (Å)	1.967(3)	1.971(5) 1.983(5)	1.964(5)
	1.975(2)	1.983(6) 1.985(6)	1.966(5)
		1.979(6) 1.982(5)	1.964(5)
		1.967(6) 1.954(6)	1.967(5)
M···N (Å)	3.648	2.980	2.965
M···C (Å)		2.738, 2.673	2.800
M···M (Å)	4.742	3.438	3.392
Ct···Ct (Å)	4.74	3.63	3.60
M.P.S. (Å)	3.33	3.21	3.19
L.S. (Å)	3.38	1.69	1.67
ΔM−N_4 plane (Å)	0	0.0219, 0.0114	0.0320

[a] Scheidt, W. R.; Turowska-Tyrk, I. *Inorg. Chem.* **1994**, *33*, 1314. [b] Olmstead, M. M.; Costa, D. A.; Maitra, K.; Noll, B. C.; Phillips, S. L.; Van Calcar, P. M.; Balch, A. L. *J. Am. Chem. Soc.* **1999**, *121*, 7090.

isostructural series, Ni^{II}(OEP), Zn^{II}(OEP), or Co^{II}(OEP). The tetragonal form of Ni^{II}(OEP) contains molecules in which the porphyrin has undergone an S_4 distortion and in which the Ni−N distances are compressed when compared to the triclinic B form of Ni^{II}(OEP) and to the Co−N distances in crystalline Co^{II}(OEP) itself.

Crystals of (μ-dioxane){Zn^{II}(OEP)}$_2$ and (py)Zn^{II}(OEP) provide five-coordinate hosts. The structure of (μ-dioxane){Zn^{II}(OEP)}$_2$, which has not been reported previously, is shown in Figure 1. In this centrosymmetric dimer, a dioxane molecule is coordinated to zinc ions in two different porphyrins with all eight ethyl groups of each porphyrin oriented to encapsulate the dioxane portion.

The complexes (py)$_2$$Zn^{II}$(OEP) and (py)$_2$$Mg^{II}$(OEP) are isostructural and provide a pair of six-coordinate hosts. The structure of (py)$_2$$Zn^{II}$(OEP), which has not previously been reported, is shown in Figure 2.

The hosts C_{60}·2Zn^{II}(OEP)·$CHCl_3$, C_{70}·Ni^{II}(OEP)·C_6H_6·$CHCl_3$, and C_{60}·Ni^{II}(OEP)·2C_6H_6 provide unusual environments in which the metalloporphyrins are sandwiched between a fullerene on one side and another metalloporphyrin on the other. The porphyrin−porphyrin contacts are close as seen in Table 1, and there are unusually short contacts between the fullerene carbon atoms and the metal ions at the centers of the porphyrins. These aspects of the structure of C_{60}·2Zn^{II}(OEP)·$CHCl_3$ are shown in Figure 3, which emphasizes the proximity of the two crystallographically distinct Zn^{II}(OEP) molecules in the solid.

Table 2 gives corresponding data for the crystalline complexes, Co^{II}(OEP),[25] C_{60}·2Co^{II}(OEP)·$CHCl_3$,[15] and C_{70}·Co^{II}(OEP)·C_6H_6·$CHCl_3$,[15] and allows the reader to compare the structural features of Co^{II}(OEP) in these environments with those of their Ni(II), Zn(II), and Mg(II) counterparts in Table 1.

EPR Spectra of Co^{II}(OEP)-Doped Hosts. EPR spectra have been collected on polycrystalline samples of the host crystals grown from solutions containing 1% or 10% Co^{II}(OEP) by the procedures previously used to obtain the undoped crystals. The spectra obtained for either level of doping are similar and show no significant variations in the observed g values or hyperfine splittings. The observation of unique EPR spectra from each of these crystals shows that Co^{II}(OEP) molecules have been introduced into the crystals, and the low level of doping ensures that the samples are magnetically dilute. The need for magnetic dilution is seen from the fact that crystalline Co^{II}(OEP) itself showed no EPR spectrum at all temperatures examined.

Figure 4 shows the EPR spectra of Co^{II}(OEP) doped into three hosts (H_2(OEP), the triclinic B form of Ni^{II}(OEP), and the tetragonal form of Ni^{II}(OEP)),which provide a four-coordinate environment for the dopant. As Figure 4 shows, there are significant differences between the spectra obtained. These variations must reflect the differing local environments within the three different crystals and the distortion that each host places upon the guest. Thus, the spectra obtained for the doped tetragonal form of Ni^{II}(OEP) show axial symmetry, which is consistent with the fact that the porphyrin is situated at a site of $\bar{4}$ symmetry. However, the spectra obtained with doped H_2(OEP), and with the doped triclinic B form of Ni^{II}(OEP), show an orthorhombic pattern that is consistent with sites that

(25) Scheidt, W. R.; Turowska-Tyrk, I. *Inorg. Chem.* **1994**, *33*, 1314.

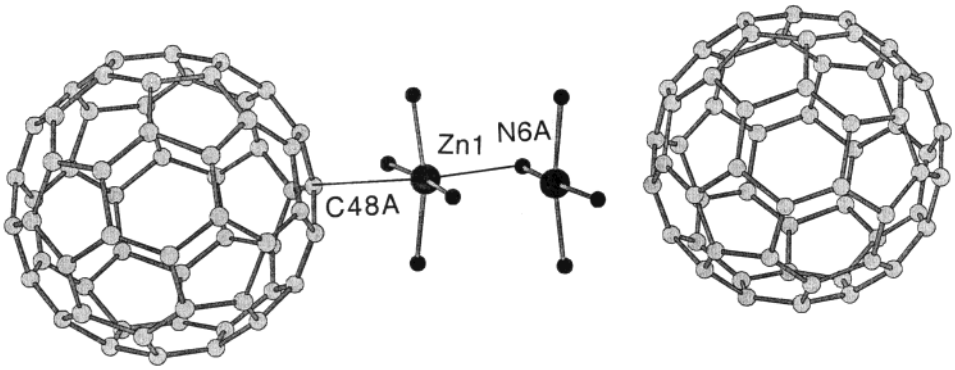

Figure 3. A view of the structure of $C_{60}{\cdot}2Zn^{II}(OEP){\cdot}CHCl_3$ (data from ref 15) which shows the two crystallographically distinct $Zn^{II}(OEP)$ molecules. There is only one fullerene in the asymmetric unit, but two fullerene molecules are displayed in the figure to show the nature of the porphyrin−fullerene interactions. The Zn1−N6A distance is 2.592 Å, and the direction Zn1−N6 deviates by only 3.6° from the normal to the least-squares plane of four nitrogen atoms coordinated to Zn1. C48A in the fullerene is 2.944 Å from Zn1, and the direction Zn1−C48A deviates by 7.2° from the normal to the N_4 plane. The angle C48A−Zn−N6A is 175.5°. The analogous relations for Zn2 are as follows: Zn2−N2A distance = 2.673 Å; the angle from the normal, 1.9°; Zn2−C6A distance = 2.984 Å, 5.5° from the normal; the C6A−Zn2−N2A angle = 176.1°.

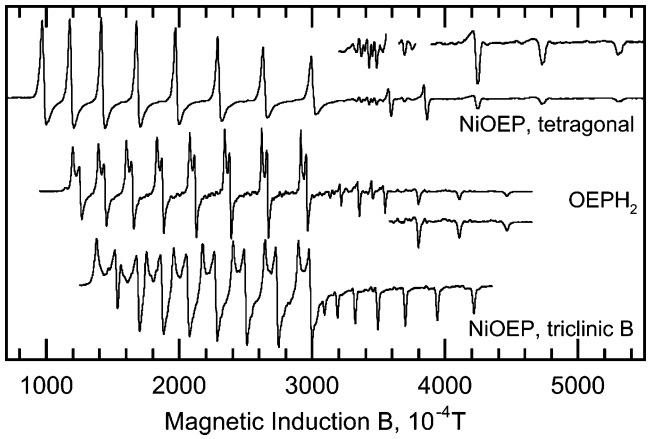

Figure 4. X-band EPR spectra (at 4.2 K) of $Co^{II}(OEP)$ doped into H_2-(OEP) (9.678 GHz), the triclinic B form of $Ni^{II}(OEP)$, and the tetragonal form of $Ni^{II}(OEP)$ (9.673 GHz).

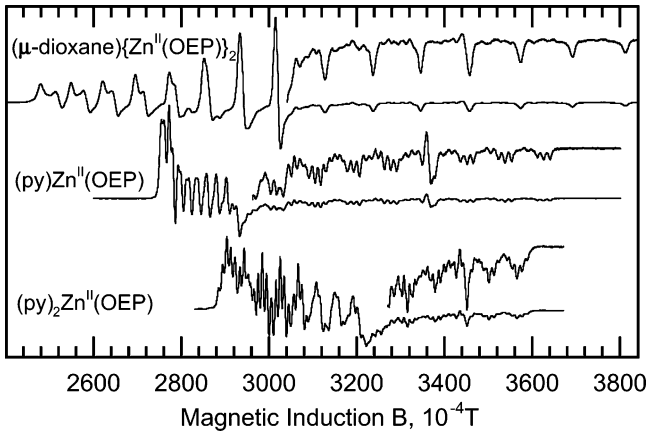

Figure 5. X-band spectra of $Co^{II}(OEP)$ doped into (μ-dioxane)$\{Zn^{II}(OEP)\}_2$ (top, 9.673 GHz), (py)$Zn^{II}(OEP)$ (center, 9.441 GHz), recorded on an ElexSys 500 Bruker spectrometer, and $(py)_2Zn^{II}(OEP)$ (bottom, 9.674 GHz). The spectra of the pyridine adducts show poorer resolution at 4.2 K, but their spectral parameters are unchanged.

have no crystallographic symmetry. Relevant EPR parameters for these and all other crystalline hosts considered here as obtained from spectral simulations (vide infra) are summarized in Table 3. Note that the spectral parameters for $Co^{II}(OEP)$ doped in the isostructural hosts, the triclinic B form of Ni^{II}-(OEP) and $Zn^{II}(OEP)$, are similar.

The powder EPR spectra of $Co^{II}(OEP)$ doped into the five-coordinate hosts, (μ-dioxane)$\{Zn^{II}(OEP)\}_2$ and (py)$Zn^{II}(OEP)$, and the six-coordinate host, $(py)_2Zn^{II}(OEP)$, are shown in Figure 5. Each spectrum shows an orthorhombic pattern that is consistent with the crystallographic sites symmetries in these hosts. The high-field resonances in the spectra obtained from doped (py)$Zn^{II}(OEP)$ show additional triplet hyperfine coupling from the axial nitrogen ligand, while such splitting is absent in the spectrum obtained for doped (μ-dioxane)$\{Zn^{II}(OEP)\}_2$. With the spectra obtained from doped $(py)_2Zn^{II}(OEP)$, the high-field lines clearly show a quintet splitting that results from the presence of two axial nitrogen ligands. The spectra obtained from doping either member of the isostructural pair, $(py)_2Zn^{II}$-(OEP) and $(py)_2Mg^{II}(OEP)$, are nearly identical as one might expect from the structural similarity.

Figure 6 shows the EPR spectra of polycrystalline samples of $C_{60}{\cdot}2Zn^{II}(OEP){\cdot}CHCl_3$, $C_{60}{\cdot}Ni^{II}(OEP){\cdot}2C_6H_6$, and $C_{70}{\cdot}Ni^{II}$-(OEP)$\cdot C_6H_6\cdot CHCl_3$ doped with $Co^{II}(OEP)$. The spectrum from $C_{70}{\cdot}Ni^{II}(OEP){\cdot}C_6H_6{\cdot}CHCl_3$ shows an orthorhombic pattern

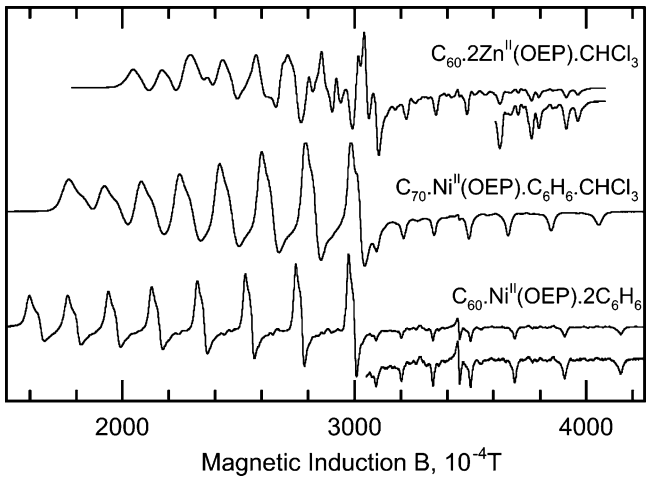

Figure 6. X-band EPR spectra at 4.2 K of polycrystalline samples of $C_{60}{\cdot}2Zn^{II}(OEP){\cdot}CHCl_3$ (9.674 GHz), $C_{60}{\cdot}Ni^{II}(OEP){\cdot}2C_6H_6$ (9.675 GHz), and $C_{70}{\cdot}Ni^{II}(OEP){\cdot}C_6H_6{\cdot}CHCl_3$ doped with $Co^{II}(OEP)$ (9.674 GHz).

which is consistent with the presence of a single porphyrin site with no crystallographically imposed symmetry. With Co^{II}-(OEP)-doped $C_{60}{\cdot}2Zn^{II}(OEP){\cdot}CHCl_3$, however, the spectrum shows that there are two independent approximately axial

Table 3. EPR Parameters for Co^{II}(OEP) Doped in Host Crystals[a]

host	g_x	g_y	g_z	10^{-4} cm^{-1} A_x	A_y	A_z	c_1	c_3	10^{-4} cm^{-1} P	κ
H_2OEP	3.235	3.317	1.785	366	378	−162[e]	0.445	0.434	279	−61[b]
						162	0.291	0.135	248	56[c]
										failed[d]
Ni^{II}(OEP) triclinic B, 4.2 K	3.031	3.207	1.879	294	324	−149[e]	0.405	0.430	252	−53[b]
						149	0.245	0.168	230	58[c]
						149	0.312	0.135	265	27[d]
Ni^{II}(OEP) triclinic B, 77 K	3.040	3.200	1.881	295	322	−148[e]	0.393	0.414	256	−48[b]
						148	0.234	0.146	255	45[c]
						148	0.285	0.103	294	11[d]
Ni^{II}(OEP) tetragonal	3.405	3.405	1.544	457	457	−202[e]	0.511	0.402	322	−91[b]
										failed[c]
										failed[d]
Zn^{II}(OEP) triclinic (4.2 K)	3.019	3.1857	1.887	289	318	−147[e]	0.388	0.409	256	−46[b]
						147	0.229	0.144	259	42[c]
						147	0.277	0.104	300	8[d]
Zn^{II}(OEP) triclinic (77 K)	3.026	3.180	1.888	290	316	−147[e]	0.388	0.411	255	−46[b]
						147	0.229	0.146	258	43[c]
						147	0.277	0.107	300	8[d]
(μ-dioxane){Zn^{II}(OEP)}$_2$	2.492	2.510	2.021	82.6	90.2	−106.3[e]	0.194	0.256	150	−29[b]
						106.3	0.083	0.140	112	57[c]
						106.3	0.092	0.136	77	68[d]
(py)Zn^{II}(OEP), 12 K	2.37	2.37	2.03	−22.7	−22.7	81.5	0.058	0.138	314	−55[c]
							0.065	0.133	253	−42[d]
(py)$_2Zn^{II}$(OEP), 35 K	2.255	2.264	2.062	−43.7	−45.4	58.2	0.034	0.177	217	−38[c]
							0.043	0.168	182	−34[d]
(py)$_2Mg^{II}$(OEP), 35 K	2.255	2.264	2.062	−43.7	−45.4	58.2	0.034	0.177	217	−38[c]
							0.043	0.168	182	−34[d]
C_{60}·2Zn^{II}(OEP)·$CHCl_3$ site 1, 4.2 K	2.575	2.575	1.998	131	131	−122[e]	0.222	0.269	189	−28[b]
						122	0.101	0.115	*−103*	*168*[c]
						122	0.110	0.110	*−56*	*150*[d]
C_{60}·2Zn^{II}(OEP)·$CHCl_3$ site 2, 4.2 K	2.710	2.710	1.9795	175	175	−127[e]	0.267	0.31	209	−29[b]
						127	0.130	0.118	*564*	*−114*[c]
						127	0.143	0.110	*4600*	*−2100*[d]
C_{60}·2Zn^{II}(OEP)·$CHCl_3$ site 1, 295 K	2.699	2.699	1.980	171	171	−126[e]	0.264	0.305	207	−28[b]
						126	0.128	0.116	*638*	*−148*[c]
						126	0.115	0.073	*−361*	*305*[d]
C_{60}·2Zn^{II}(OEP)·$CHCl_3$ site 2, 295 K	2.780	2.780	1.960	200	200	−126[e]	0.291	0.325	217	−27[b]
						126	0.147	0.107	**429**	**−58**[c]
						126	0.162	0.090	*723*	*−220*[d]
C_{70}·Ni^{II}(OEP)·C_6H_6·$CHCl_3$	2.816	2.890	1.944	218	235	−136[e]	0.314	0.344	233	−34[b]
						136	0.165	0.108	337	−8[c]
						136	0.183	0.086	**458**	**−81**[d]
C_{60}·Ni^{II}(OEP)·2C_6H_6	2.955	2.999	1.908	266	274	−145[e]	0.353	0.274	250	−41[b]
						145	0.198	0.107	290	21[c]
						145	0.224	0.060	347	−19[d]

[a] Italic type represents unacceptable results because of the magnitude of P, over 500 or negative. Bold type represents barely acceptable results, P over 350. Failed means that the g values could not be reproduced. [b] From McGarvey's formulas 31−34 (ref 6), unpaired electron in xy. [c] From McGarvey's third-order formulas 27−30 (ref 6), unpaired electron in z^2. [d] From Mcgarvey's "exact" formulas 48−56 (ref 6), unpaired electron in z^2. [e] Sign determined from theoretical fit of spectra not from experiment.

patterns which are particularly apparent in the high-field region. These two orthorhombic resonances arise from the presence of two crystallographically distinct porphyrin sites within this solid.

To better understand the origin of the EPR resonances of Co^{II}(OEP) doped into C_{60}·2Zn^{II}(OEP)·$CHCl_3$, single-crystal spectra have been obtained at 4.2 K. Relevant data are shown in Figure 7. When a single-crystal of Co^{II}(OEP)-doped C_{60}·2Zn^{II}(OEP)·$CHCl_3$ was rotated about the crystallographic a axis, the "inner" spectrum (with a larger g_z and smaller $g_{x,y}$ values than in the "outer" spectrum) passed through its high-field turning point (with the minimal g effective, nearly equal to g_z) at ±24° from the crystallographic c axis, while the "outer" spectrum passed the turning point (with its g effective at the minimum, nearly equal to g_z) at ±26° from the c axis. The orientations of a crystal where the magnetic field is parallel to either b or c are easily recognized during the rotation, because the spectra of the symmetry-equivalent sites exactly overlap as seen in Figure 7. We expect that the z axis of the Co^{II}(OEP) molecule is perpendicular to the least-squares plane of four nitrogen atoms. The z axes at the sites of Zn1 and Zn2 defined in this way are nearly perpendicular to the crystallographic a axis (89.4°) and form angles of 24.5° and 26.3°, respectively, with the c axis as calculated from the crystal structure. Therefore, we can assign the "inner" spectrum to the Zn1 site and the "outer" spectrum to the Zn2 site. The EPR parameters of Co^{II}(OEP)-doped C_{60}·2Zn^{II}(OEP)·$CHCl_3$ were significantly temperature dependent, and spectra could be observed at all temperatures. Spectral parameters of data collected at 4.2 and 295 K are given in Table 3.

Although the crystals used in this work were handled in air, there was no evidence of characteristic EPR spectra of the dioxygen adducts[1,2,6,7] of Co^{II}(OEP) from our samples. The compact nature of the molecular packing within the crystals appears to preclude entry of dioxygen.

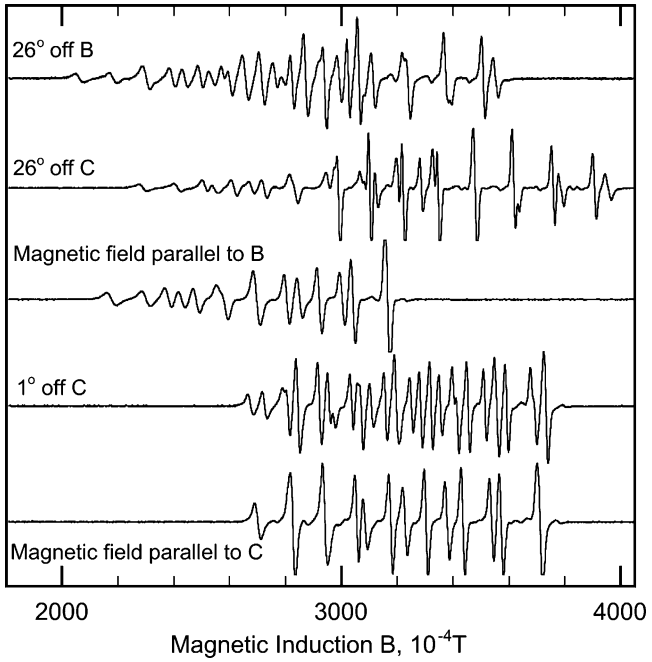

Figure 7. Single-crystal EPR spectra of Co^{II}(OEP)-doped C_{60}·2Zn^{II}(OEP)·$CHCl_3$ (9.680 GHz, 8.0 K). With the magnetic field parallel to either the crystallographic *b* or the crystallographic *c* axis, the spectra of the symmetry-equivalent sites exactly overlap, but they clearly split at only 1° off the axes. The "outer" spectrum, which is associated with the Zn2 site, passes through its low-field and high-field turning point at the orientations ±26° off the *b* axis and ±26° off the *c* axis, respectively. The spectra of Co^{II}(OEP) at the Zn1 site pass through the turning points at ±24.5° off the *b* and *c* axes (not shown).

Simulations of the EPR Spectra. Assuming that the *g* and *A* tensors of the cobalt ion are coaxial, as confirmed by our single-crystal spectra, the spin Hamiltonian has the form:

$$\hat{H} = \mu_\beta(g_x B_x \hat{S}_x + g_y B_y \hat{S}_y + g_z B_z \hat{S}_z) + A_x \hat{S}_x \hat{I}_x + A_y \hat{S}_y \hat{I}_y + A_z \hat{S}_z \hat{I}_z \quad (1)$$

The energy levels of a spin system and the resonance fields corresponding to that Hamiltonian are commonly evaluated by using the second-order perturbation calculation. In the present work, this proved to be inadequate because some of the hyperfine splittings (particularly in the case of Co^{II}(OEP) doped in tetragonal Ni^{II}(OEP)) are very large. A new simulation program was developed that employed the exact diagonalization of the 16 × 16 complex spin Hamiltonian matrix to calculate the energy levels at an arbitrary orientation of a molecule. The resonance fields were found by iterative procedures. Matrix diagonalization was accomplished by the Householder method.[26] Transition probabilities were calculated from the eigenvectors as described previously.[27] The spectra of polycrystalline samples were simulated as superpositions of many single-crystal spectra. The method gave strikingly good simulations in difficult cases. For example, Figure 8 compares the experimental spectrum obtained for Co^{II}(OEP) doped into the tetragonal form of Ni^{II}(OEP) with the simulated spectrum. In this case, the large value of the cobalt hyperfine coupling produces spectral features that are not satisfactorily handled by the perturbation calculation.

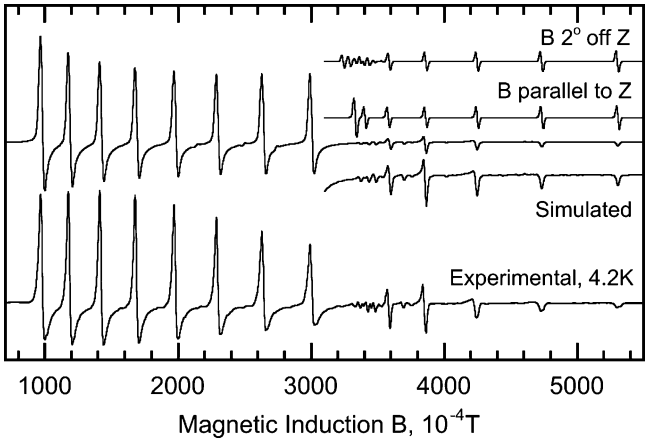

Figure 8. Experimental (4.2 K) and simulated spectra of Co^{II}(OEP) doped into the tetragonal form of Ni^{II}(OEP) (9.676 GHz). Note that the low-intensity signals around 3400 G are a part of the "parallel" hyperfine pattern of Co^{II}(OEP) and that only two highest-field parallel lines show the normally expected shape due to the unusually large hyperfine splitting. In the inset showing the spectrum simulated with the magnetic field parallel to *z*, two low-field lines overlap as a result of the extremely uneven spacing between the hyperfine components. At the orientation 2° off the *z* axis, the forbidden transitions become visible. (They are strictly forbidden at axial orientations.)

The components of the *g* and *A* tensors for all samples examined here are given in Table 3.

Discussion

The results presented here demonstrate that Co^{II}(OEP) can be introduced into a variety of different crystals and that the EPR spectra of these doped samples are very sensitive to the environment within each crystal. Although the Co^{II}(OEP) molecule has axial symmetry, it displays either axial or rhombic EPR resonances when incorporated into crystalline hosts. The crystallographic site symmetry determines whether these axial or rhombic resonance patterns are observed. Moreover, in C_{60}·2Zn^{II}(OEP)·$CHCl_3$ where two different metalloporphyrin sites are present,[15] two different patterns of rhombic EPR resonances have been resolved. Thus, the EPR spectrum of Co^{II}(OEP) in a particular host crystal is sensitive to its environment.

Although it might be expected that Co^{II}(OEP) can undergo isomorphic replacement into hosts that are isostructural with those of known Co^{II}(OEP) derivatives such as crystalline Co^{II}(OEP) itself, C_{60}·2Co^{II}(OEP)·$CHCl_3$, and C_{70}·Co^{II}(OEP)·C_6H_6·$CHCl_3$ (see Table 2), the data show that Co^{II}(OEP) can be incorporated into hosts for which the corresponding structure of a cobalt complex does not exist. While the later statement may simply reflect the fact that hypothetical compounds such as "(py)Co^{II}(OEP)", "(py)$_2$$Co^{II}$(OEP)", and "($\mu$-dioxane){$Co^{II}$(OEP)}$_2$" have not yet been prepared,[28−30] it is more significant that Co^{II}(OEP) can be incorporated into the tetragonal form of Ni^{II}(OEP), which has a significantly distorted geometry of the porphyrin that usually is thought to reflect the small size of Ni(II).

While the EPR parameters of Co(II) porphyrins in five- and six-coordinate forms have received considerable attention previ-

(26) Wilkinson, J. H. *The Algebraic Eigenvalue Problem*; Clarendon Press: London, 1970.
(27) Bencini A.; Gatteschi, D. In *Transition Metal Chemistry*; Melson, G. A., Figgis, B. N., Eds.; Marcel Dekker: New York 1982; Vol. 8, p 1.
(28) The related five- and six-coordinate complexes, (4-Me$_2$N-py)Co^{II}(OEP) with Co−N (equitoral) 1.982(2), Co−N (axial) 2.191(2) Å,[29] and (3-Me-py)$_2$$Co^{II}$(OEP) with Co−N(equatorial) 1.991(1) and 1.993(1) Å, Co−N (Axial) 2.386(2) Å,[30] have, however, been crystallized, and their structures were determined.
(29) Summers, J. S.; Petersen, J. L.; Stolzenberg, A. M. *J. Am. Chem. Soc.* **1994**, *116*, 7189−7195.
(30) Little, R. G.; Ibers, J. A. *J. Am. Chem. Soc.* **1974**, *96*, 4440.

ously, the range of spectra seen here for Co^{II}(OEP) in what are nominally four-coordinate environments in H_2(OEP), the triclinic B form of Ni^{II}(OEP), and the tetragonal form of Ni^{II}(OEP) and in the fullerene cocrystals is significant.

Interpretation of the EPR Parameters for Four-Coordinate Co^{II}(OEP). Cobalt porphyrin complexes with axially coordinated ligands are known to have the $^2A_1(z^2)$ ground states. The $^2A_1(z^2)$ state also has been also often assumed correct for four-coordinate cobalt(II) porphyrins. The components of the g tensor may be calculated from the formulas derived by McGarvey through the use of a third-order perturbation calculation where the contribution due to the low-lying quartet states is taken into account.[6] In that approach, the multielectron ground term for Co(II) is written as the determinantal wave function:

$$^2A_1^{\pm} = (d_{xz})^2(d_{yz})^2(ad_{xy}^{\pm} - bd_{z^2}^{\pm})^2(bd_{xy}^{\pm} + ad_{z^2}^{\pm}) \qquad (2)$$

Coefficients a and b reflect the mixing of the xy and z^2 orbitals in symmetries lower than C_{4v}, while in higher symmetry either a or b must equal 0.[6,31]

Formulas for g adapted for the axially symmetrical case with the $^2A_1(z^2)$ ground state and $a = 1$, $b = 0$ (unpaired electron on z^2) are

$$g_{\perp} = 2.0023 + 6c_1 - 6c_1^2 + 2c_3^2$$

$$g_{||} = 2.0023 - 3c_1^2 + 2c_3^2 \qquad (3)$$

where it was assumed that the states ^4E and $^4A_2$ are close in energy ($c_5 = c_3$).[32]

$$c_1 = \frac{\lambda}{\Delta E_{^2A_1 \leftarrow {}^2E}}$$

$$c_3 = \frac{\lambda}{\Delta E_{^2A_1 \leftarrow {}^4E}}$$

Thus, the coefficients c_1 and c_3 can be found from the g values only. From the cobalt hyperfine coupling constants, the Fermi contact term κ and the anisotropic term P can then be calculated:

$$A_{x,y} = \kappa + P\{-2/7 + (45/7)c_1 + (2/7)c_3 + (4/21)c_3^2 + (40/63)c_5^2 - (57/14)c_1^2 - (34/21)c_5c_3\}$$

$$A_z = \kappa + P\{4/7 - (4/7)c_3 - (6/7)c_1 + (2/63)c_3^2 - (64/63)c_5^2 + (15/7)c_1^2 + (8/21)c_5c_3\} \qquad (4)$$

For Co^{II}(OEP) doped into tetragonal Ni^{II}(OEP), however, the system of equations for the g components given above has no solution. (In the examples treated in the original paper by McGarvey, none of the complexes exhibited such high $g_{x,y}$ values and such low g_z values as those reported here for Co^{II}-(OEP) doped into tetragonal Ni^{II}(OEP).) Moreover, the "exact" solutions obtained from the diagonalization of the energy matrix (formulas 48−56 in ref 6) also cannot reproduce the experimental g values. The assumption of $b = 1$, $a = 0$ in the wave function (2), implying that the unpaired electron is in the xy orbital, results in the expressions (eqs 31−34 in ref 6)

$$g_{x,y} = 2.0023 + (2/3)c_3(c_3 + 2c_1) + 2c_1$$

$$g_z = 2.0023 - 3c_1^2 + 2c_3^2 - 8c_6$$

$$A_{x,y} = \kappa + P\{2/7 + (11/7)c_1 + (2/7)c_3 + (9/14)c_1^2 + (34/21)c_1c_3\}$$

$$A_z = \kappa + P\{-4/7 - (4/7)c_3 + (6/7)c_1 - 8c_6 + (2/7)c_3^2 - c_1^2 + (8/7)c_1c_3\} \qquad (5)$$

The equations for the g components for Co^{II}(OEP) doped into tetragonal Ni^{II}(OEP) can now be solved in terms of the coefficients c_1 and c_3, and then the values of $P = 322 \times 10^{-4}$ cm^{-1} and $\kappa = -91 \times 10^{-4}$ cm^{-1} are found from the hyperfine constants. The P value for free Co(II) ion is 254×10^{-4} cm^{-1},[33] and the result seems to be reasonable, because higher values were accepted in the literature.[6] In these calculations, it was necessary to assume that A_z was negative. In the case of the d_{xy} ground state, the g and A values become dependent on one more unknown parameter, c_6, that reflects the energy difference between xy and $x^2 - y^2$ orbitals. The $x^2 - y^2$ orbital in cobalt porphyrins is known to be much higher in energy than all of the remaining d orbitals, and thus c_6 is expected to be much smaller than c_1. In a series of calculations where c_6 was allowed to vary over the range from 0 to $0.5c_1$, we found that the lowest c_6 values gave the most reasonable results.

If a sensible value of P is used as a criterion of the quality of the method, then the EPR parameters of all compounds without axial ligands considered in Table 3 are more satisfactorily explained by placing the unpaired electron in the xy orbital. Previously, Lin pointed out that the z^2 ground state in cobalt porphyrins without the axial ligand was not fully established.[18] The results of calculations by using McGarvey's third-order and for the "exact" formulas for the z^2 case and for the xy case are presented in Table 3. For samples that show nonaxial EPR parameters, average values of g_x, g_y and of A_x, A_y were used in calculations, because the differences between the equatorial EPR parameters are small as compared to the large differences between the equatorial and the axial EPR parameters. Considering the x and y parameters separately results in more data that could be fit, but also requires additional c coefficients. From the data in Table 3, it is seen that the assumption of the z^2 as the orbital housing the unpaired electron results in many cases in unacceptable values of the hyperfine term P. In contrast, a smooth trend that parallels the changes in g is observed for all samples except the five- and six-coordinate complexes if the xy orbital is assumed to be the orbital holding the unpaired electron. For the five- and six-coordinate complexes, the presence of hyperfine coupling to the axial ligands is consistent with z^2 as the orbital housing the unpaired electron. Such coupling would not be seen if the xy orbital contained the unpaired electron, because the axial ligands would then lie in nodal planes of the spin-containing orbital. Table 3 shows that the term κ is calculated to be negative for all samples if we use

(31) Note that in this paper the $x^2 - y^2$ orbital points toward the four porphyrin nitrogen atoms. This orientation is the one usually used in metalloporphrins, but in the original McGarvey paper[6] the orbital designations of xy and $x^2 - y^2$ have been swapped with xy pointing toward the porphyrin nitrogen atoms.

(32) Wayland, B. B.; Sherry, A. E.; Bunn, A. G. *J. Am. Chem. Soc*. **1993**, *115*, 7675.

(33) McGarvey, B. R. *J. Chem. Phys*. **1967**, *71*, 51

the equation set 5 where applicable (see above). Also, the variation in magnitude of κ is relatively small. When the unpaired electron is considered to reside on z^2 and formulas 3 and 4 are used, considerable scatter is observed in both the magnitude and the sign of κ (see Table 3 and ref 6). Because our samples cover the entire range of the EPR parameters known in low-spin cobalt(II) systems, it seems likely that κ for cobalt is always negative. This is perhaps an important result of our work.

EPR Parameters for Five- and Six-Coordinate Co^{II}(OEP). Upon addition of axial ligands, the EPR parameters of a Co(II) porphyrin change so that $g_\perp$ typically decreases to values down to 2.3, while $A_\perp$ becomes very small, for example, 10×10^{-4} cm^{-1}. Although the EPR spectrum of $(py)_2Co^{II}$(tetra(*p*-carboxyphenylporphyrinate) in a pyridine glass has axial symmetry,[1,2] its spectral parameters are otherwise similar to those of Co^{II}(OEP) doped into either $(py)_2Zn^{II}$(OEP) or $(py)_2Mg^{II}$(OEP) which have rhombic spectra. The spectral parameters reported for $(py)_2Co^{II}$(tetra(*p*-carboxyphenylporphyrinate) are $g_\perp = 2.236$, $g_\| = 2.054$, $A_\perp = 54 \times 10^{-4}$, and $A_\| = 53 \times 10^{-4}$ cm^{-1}, with additional hyperfine coupling to two axial nitrogen atoms ($A_\perp = 10 \times 10^{-4}$ and $A_\| = 12 \times 10^{-4}$ cm^{-1}). Likewise, the spectral parameters for Co^{II}(OEP) doped in $(py)Zn^{II}$(OEP) are similar to those obtained by Walker for $(py)Co^{II}$(TPP) in a toluene glass which also shows an axial spectrum with $g_\perp = 2.324$, $g_\| = 2.027$, $A_\perp = 13 \times 10^{-4}$, and $A_\| = 78.9 \times 10^{-4}$ cm^{-1} and additional hyperfine coupling from one axial nitrogen atom ($A_\| = 14.2 \times 10^{-4}$ cm^{-1}).[1,2] For the spectrum of Co^{II}(OEP) doped in (μ-dioxane)$\{Zn^{II}(OEP)\}_2$, the larger spread in *g* values and the larger cobalt hyperfine coupling constants are probably a reflection of weaker bonding to the axial oxygen ligand.

EPR Parameters for Co^{II}(OEP)/Fullerene Cocrystals. Considerable attention has been given to the ability of fullerenes and metalloporphyrins to associate and cocrystallize.[15,16,34−40] The interaction between the fullerenes and the porphyrins has been considered to involve charge-transfer with the fullerene acting in a conventional electron acceptor mode or as an electron donor as well as van der Waals forces.

The *g* and *A* parameters of the fullerene adducts appear to be intermediate between the four-coordinate cobalt porphyrin complexes and the five- and six-coordinate adducts. The differences in the EPR parameters for Co^{II}(OEP) in the four-coordinate hosts versus the fullerene adducts almost certainly result from interactions of the cobalt ions with the adjacent porphyrin or the adjacent fullerene. In the fullerene adducts, a nitrogen atom from one M^{II}(OEP) moiety can occupy an axial position above the metal atom in a neighboring M^{II}(OEP) moiety.

Thus, in $C_{60}\cdot 2Zn^{II}(OEP)\cdot CHCl_3$, the zinc ion is pulled out of the plane of the porphyrin by 0.1605 or 0.1402 Å at the two different porphyrin sites toward the nitrogen atom in adjacent porphyrin and away from the fullerene. As a consequence, the axial Zn−N distances are 2.592 and 2.674 Å in sites 1 and 2, respectively. These distances are somewhat longer than the Zn−N distance (2.4039(14) Å) in $(py)_2Zn^{II}$(OEP) but do appear to signal a degree of donor/acceptor interaction between the adjacent porphyrins. This interaction is likely to be responsible for altering the EPR parameters of the doped crystals so that the *g* and *A* values lie between those observed for the more strictly four-coordinate complexes and those with five- and six-coordination. However, the interaction of the cobalt ion with the nearby nitrogen does not produce detectable nitrogen hyperfine splitting in the EPR spectrum, whereas such coupling is clearly present in the true five- and six-coordinate compounds. Notice also that the spectral parameters for Co^{II}(OEP) doped into site 1, which is the site with the shorter axial Zn−N distance, approach those of five- and six-coordinate adducts more closely than those for Co^{II}(OEP) doped into site 2, which is further from the adjacent porphyrin. In contrast, the Zn−C distances to the neighboring fullerenes are longer, 2.944 and 2.984 Å, and the interaction with the fullerene may be less important in influencing the EPR spectral parameters.

In $C_{70}\cdot Ni^{II}(OEP)\cdot C_6H_6\cdot CHCl_3$, the situation is reversed with the nickel ion 2.836 Å from the closest carbon atom of the fullerene and 3.152 Å from the nitrogen atom of the adjacent porphyrin. In $C_{60}\cdot Ni^{II}(OEP)\cdot 2C_6H_6$, the adjacent porphyrins separate even more, while the fullerene remains close to the Ni^{II}(OEP) molecule with a separation of 3.004 Å between Ni and the closest fullerene carbon atom. Thus, as the porphyrin−porphyrin distance increases and the porphyrin−fullerene distance also increases, the EPR parameters for Co^{II}(OEP) doped in $C_{70}\cdot Ni^{II}(OEP)\cdot C_6H_6\cdot CHCl_3$ and in $C_{60}\cdot Ni^{II}(OEP)\cdot 2C_6H_6$ show changes that include an increase in the Co hyperfine coupling and an increase in the range of *g* values. These changes are indicative of an alteration of the local environments that become more like those of strictly four-coordinate porphyrins.

We have attempted to utilize two versions of Lin's method[18,19] to interpret the EPR parameters in Table 3. However, while the method was able to fit the *g* and *A* values in typical four-, five-, and six-coordinate complexes, we found it inapplicable to the fullerene adducts.

EPR parameters similar to those of the fullerene adducts reported here have rarely been observed. However, Co^{II}Pc (Pc is the dianion of phthalocyanine) doped into β-Zn^{II}Pc and β-Ni^{II}Pc does exhibit *g* and *A* values[41] that are somewhat similar to those of Co^{II}(OEP) doped into $C_{60}\cdot 2Zn^{II}(OEP)\cdot CHCl_3$ and into other fullerene adducts reported in this work. In the β-form of Zn^{II}Pc, a nitrogen atom of one Zn^{II}Pc moiety is situated in an axial site above the adjacent Zn^{II}Pc with a $Zn\cdots N_{axial}$ distance of 3.23 Å.[42] Thus, there are structural similarities in the proximity of the macrocycles in β-Zn^{II}Pc and β-Ni^{II}Pc and in the fullerene adducts considered here.

Nitrogen Hyperfine Coupling. The hyperfine splitting of the pyrrole nitrogens in four-coordinate Co^{II}(TPP) doped in Zn^{II}(TPP) revealed that the three components A_x, A_y, A_z are very close to each other (although the signs are unknown): 3.1, 3.1,

(34) Boyd, P. D. W.; Hodgson, M. C.; Rickard, C. E. F.; Oliver, A. G.; Chaker, L.; Brothers, P. J.; Bolskar, R. D.; Tham, F. S.; Reed, C. A. *J. Am. Chem. Soc.* **1999**, *121*, 10487.
(35) Evans, D. R.; Fackler, N. L. P.; Xie, Z.; Richard, C. E. F.; Boyd, P. D. W.; Reed, C. A. *J. Am. Chem. Soc.* **1999**, *121*, 8466.
(36) Konarev, D. V.; Neretin, I. S.; Slovokhotov, Y. L.; Yudanova, E. I.; Drichko, N. V.; Shul'ga, Y. M.; Tarasov, B. P.; Gumanov, L. L.; Batsanov, A. S.; Howard, J. A. K.; Lyubovskaya, R. N. *Chem.-Eur. J.* **2001**, *7*, 2605.
(37) Konarev, D. V.; Yudanova, E. I.; Neretin, I. S.; Slovokhotov, Y. L.; Lyubovskaya, R. N. *Synth. Met.* **2001**, *121*, 1125.
(38) Konarev, D. V.; Kovalevsky, A. Y.; Li, X.; Neretin, I. S.; Litvinov, A. L.; Drichko, N. V.; Slovokhotov, Y. L.; Coppens, P.; Lyubovskaya, R. N. *Inorg. Chem.* **2002**, *41*, 3638.
(39) Sun, D.; Tham, F. S.; Reed, C. A.; Boyd, P. D. W. *Proc. Natl. Acad. Sci. U.S.A.* **2002**, *99*, 5088.
(40) Sun, D.; Tham, F. S.; Reed, C. A.; Chaker, L.; Boyd, P. D. W. *J. Am. Chem. Soc.* **2002**, *124*, 6604.
(41) Assour, J. M.; Kahn, W. K. *J. Am. Chem. Soc.* **1965**, *87*, 207.
(42) Scheidt, W. R.; Dow, W. *J. Am. Chem. Soc.* **1977**, *99*, 1101.

and 3.6 MHz.[5] Similarly, the pyrrole nitrogen hyperfine splitting observed in low-spin $[(PhNC)_2Fe^{III}(OEP)]^+$ which has a half-occupied *xy* orbital is 3.3 MHz with little anisotropy.[43] The hyperfine constants for $V^{IV}O$(TPP) (which also has an *xy* ground state) in Zn^{II}TPP matrix were first reported to be 9.6, 2.9, 7.9 MHz (from ENDOR)[44] and later 6.7, 7.2, 7.7 MHz (from ESEEM).[45] VO^{IV}(OEP) showed similar parameters (ESEEM).[45] The hyperfine parameters for these $V^{IV}O$ complexes are larger than those of Co^{II}(TPP), but both in Co and in V they imply only a very small spin population on the nitrogen orbitals. According to McGarvey, quite large nitrogen hyperfine constants (~15 MHz) from the in-plane pyrrole donors should be expected for the z^2 ground orbital,[6] but this has never been observed. For example, the anisotropic hyperfine splittings of the pyrrole nitrogens in (py)Co^{II}(TPP) where the z^2 orbital is half-occupied were found to 2.4, 2.9, and 4.1 MHz in frozen toluene solution.[4]

Experimental Section

Materials. Octaethylporphyrin, $OEPH_2$, was purchased from Mid Century and used without purification. Ni^{II}(OEP), Co^{II}(OEP), and Zn^{II}(OEP) were prepared by reacting metal acetates with $OEPH_2$ in glacial acetic acid.[46] The fullerene-containing crystals were obtained as described previously.[15] Doped crystals were obtained by crystallizing the desired host from solution in the presence of 10% or 1% Co^{II}(OEP). No significant differences in EPR spectra of the samples doped at the 10% level versus those doped at 1% level were observed. Attempts to obtain a doped sample of the triclinic form A of Ni^{II}(OEP) by the published method[47] failed.

EPR Spectra. The X-band EPR spectra were recorded on a Bruker ECS-106 instrument equipped with an Oxford Instruments variable-temperature liquid helium cryostat. The microwave frequency was measured by using a calibrated cavity resonator, and the magnetic field intensity was checked using solid DPPH as a standard. A Bruker single-axis goniometer was used for single-crystal measurements. Spectra of all samples were recorded at 4.2 K. In addition, the spectra were obtained at higher temperatures where possible. The mono- and di-pyridine adducts, (py)Zn^{II}(OEP), $(py)_2Zn^{II}$(OEP), and $(py)_2Mg^{II}$(OEP), were measured at temperatures of 12 and 35 K, respectively, because the spectra showed somewhat better resolution at these temperatures than at 4.2 K. Most samples exhibited EPR signals only at low temperatures, but the spectra of doped C_{60}·2Zn^{II}(OEP)·$CHCl_3$, C_{70}·Ni^{II}(OEP)·C_6H_6·$CHCl_3$, and of pure C_{70}·Co^{II}(OEP)·C_6H_6·$CHCl_3$ could be observed at all temperatures. Pure samples of crystalline Co^{II}(OEP) itself showed no EPR spectrum at all temperatures examined.

Crystal Growth. Samples of (μ-dioxane){Zn^{II}(OEP)}$_2$ suitable for X-ray diffraction were obtained by slow evaporation of a Zn^{II}(OEP) solution in dioxane containing traces of pyridine. Crystals of $(py)_2Zn^{II}$-(OEP) were grown from a solution of Zn^{II}(OEP) in a 1:1 mixture of dioxane and pyridine.

X-ray Data Collection. The crystals were removed from the glass tube together with a small amount of mother liquor and immediately coated with a hydrocarbon oil on a microscope slide. A suitable crystal was mounted on a glass fiber with silicone grease and placed in the cold stream of a Bruker SMART CCD with graphite monochromated Mo Kα radiation at 90(2) K. Lorentz and polarization corrections were applied. No decay was observed in 50 duplicate frames at the end of the data collection. An empirical absorption correction utilizing equivalents was employed.[48] Crystal data are reported in Table 4.

Table 4. Crytal Data and Data Collection Parameters

	Zn^{II}(OEP)	{(μ-dioxane){Zn^{II}(OEP)}$_2$	$(py)_2Zn^{II}$(OEP)
formula	$C_{36}H_{44}N_4Zn$	$C_{76}H_{96}N_8O_2Zn_2$	$C_{46}H_{54}N_6Zn$
formula weight	598.12	1284.35	756.32
color and habit	red rod	red prism	red prism
crytal system	triclinic	monoclinic	triclinic
space group	$P\bar{1}$	$P2_1/n$	$P\bar{1}$
a, Å	4.692(4)	14.9979(11)	9.8564(9)
b, Å	13.185(10)	9.7677(9)	10.3391(10)
c, Å	13.287(10)	22.930(2)	10.4252(11)
α, deg	113.94(3)	90	98.970(5)
β, deg	91.177(15)	90.021(3)	90.724(4)
γ, deg	92.157(14)	90	114.565(5)
V, Å^3	750.1(10)	3359.2(5)	950.87(16)
T, K	90(2)	90(2)	90(2)
Z	1	2?	1
d_{calcd}, g cm^{-3}	1.324	1.270	1.321
radiation (λ, Å)	Mo Kα (0.71073)	Mo Kα (0.71073)	Mo Kα (0.71073)
μ, mm^{-1}	0.851	0.767	0.688
range of transm. factors	0.58−0.90	0.89−0.93	0.65−0.84
no. of unique data	4192	8314	4211
no. of restraints	0	0	0
no. of params. refined	188	406	245
R1[a]	0.035	0.041	0.042
wR2[b]	0.090	0.106	0.143

[a] For data with $I > 2\sigma I$. R1 = $(\sum||F_o| - |F_c||)/\sum|F_o|$. [b] For all data. wR2 = $\sqrt{\sum[w(F_o^2-F_c^2)^2]/\sum[w(F_o^2)^2]}$.

Solution and Structure Refinements. Calculations for the structures were performed using SHELXS-97 and SHELXL-97. Tables of neutral atom scattering factors, f' and f'', and absorption coefficients were taken from a standard source.[49] The structures were solved by direct methods. All atoms except hydrogen atoms were refined anisotropically. All hydrogen atoms were located in difference Fourier maps and included through the use of a riding model.

Acknowledgment. We thank the National Science Foundation (grant CHE 0070291) and the National Institutes of Health (grant GM26226) for support, and Dr. M. M. Olmstead for asssistance. The Bruker SMART 1000 diffractometer was funded in part by NSF Instrumentation grant CHE-9808259.

Supporting Information Available: Crystallographic details (CIF). This material is available free of charge via the Internet at http://pubs.acs.org.

JA030221F

(43) Astashkin, A. V.; Raimsimring, A. M.; Kennedy, A. R.; Shokhireva, T. Kh.; Walker, F. A. *J. Phys. Chem. A* **2002**, *106*, 74.
(44) Mulks, C. F.; van Willigen, H. *J. Phys. Chem*. **1981**, *85*, 1220.
(45) Fukui, K.; Ohya-Nigiguchi, H.; Kamuda, H. *J. Phys. Chem.* **1993**, *97*, 11858.
(46) Dorough, G. D.; Miller, J. R.; Huennekens, F. M. *J. Am. Chem. Soc*. **1951**, *73*, 4315.
(47) Cullen, D. L.; Meyer, E. F., Jr. *J. Am. Chem. Soc*. **1974**, *96*, 2095.
(48) SADABS (G. M. Sheldrick) based on a method of: Blessing, R. H. *Acta Crystallogr., Sect. A* **1995**, *A51*, 33.
(49) *International Tables for Crystallography*; Wilson, A. J. C., Ed.; Kluwer Academic Publishers: Dordrecht, 1992; Vol. C.